Decorrelating density and drag-coefficient through attitude variations

Vishal Ray
University of Colorado Boulder
Daniel J. Scheeres
University of Colorado Boulder

Suood Alnaqbi
University of Colorado Boulder

ABSTRACT

An accurate estimation of upper atmospheric densities is crucial for precise orbit determination and prediction of low Earth orbit (LEO) satellites as well as scientific studies of the Earth's atmosphere. But densities derived using satellite tracking data are always uncertain up to the drag-coefficient that is assumed in the inversion method. In this work, we develop a framework to simultaneously estimate the density and drag-coefficient for satellites with time-varying attitude leveraging Fourier drag-coefficient models. The method is tested with synthetic data for different geomagnetic activities and validated with actual POD from Spire satellites.

1. INTRODUCTION

In 1957, with the launch of Sputnik 1, a new era began for humanity - the space age. Since then, satellite technology has permeated almost every aspect of our lives, revolutionizing the way modern society functions. The protection of our world's collective space assets is a shared interest to all of humanity. As with the discovery of any new resource, swift utilization without a lot of thought dedicated to sustainability due to the seeming abundance of given resource was what happened to outer space as well. In the nearly 65 years following the launch of the first satellite, we have added more than 23000 objects that are more than 10 centimeters in size [1]; and that is just the number of objects that are being tracked and cataloged for collision avoidance purposes. With the object population in certain low Earth orbit (LEO) belts reaching a critical spatial density [2], accurate real-time monitoring as well as prediction of satellite positions into the future has emerged as a problem of utmost importance for orbit maintenance and collision avoidance. The relevance of tracking accuracy is underscored by the 2009 collision between a Kosmos and an Iridium satellite. In recent years, with the launch of mega-constellations of commercial satellites such as SpaceX's Starlink, the number of near-misses that would increase the debris population by thousands of more objects has been quickly rising, especially in the absence of traffic rules, communication protocols between different satellite operators and the potential lack of transparency regarding conjunction events [3]. Along with active debris remediation strategies and developing policies regarding norms of behaviour in space, improving tracking accuracy of space objects is necessary to prevent catastrophic collisions of active maneuverable satellites.

The modeling of perturbing forces acting on a satellite is a key component of orbit determination and prediction. Atmospheric drag is the largest perturbing force for low altitude LEO satellites and uncertainty in its parameters remains the foremost contributor of prediction errors in this orbit regime [4]. Even though high-fidelity non-conservative force models used in conjunction with empirical accelerations meet current requirements in terms of orbit fit residuals, the prediction accuracy may still degrade rapidly due to inherent assumptions in the modeling and estimation of force parameters such as the drag coefficient [5].

In the orbit determination process, the atmospheric density is usually modeled in the filter using semi-empirical models calibrated with satellite data and the drag-coefficient is estimated as a constant. But significant discrepancies exist between the current operational semi-empirical density models [6] such as NRLMSISE-00 [7], JB2008 [8] and DTM-2013 [9] due to the differences in calibration data as well as physics of the models. Any errors in the atmospheric

density will consequently get absorbed in the estimated states and drag-coefficient, leading to errors in predicted orbits.

In an ideal scenario, one would utilize an atmospheric density model that is calibrated real-time using tracking data from multiple satellites such as the Air Force High Accuracy Satellite Drag Model (HASDM) [10] in order to reduce errors due to atmospheric density and obtain physically consistent values of the drag coefficient. But unfortunately, HASDM is not available to users outside of the Department of Defense. Data-assimilation methods for physics-based atmospheric models have been proposed to estimate the global atmospheric density [11, 12, 13]. These methods combine the advantages of physics-based models in their ability to account for the thermospheric dynamics and provide density forecasts, and indirect measurements of the actual state of the thermosphere via data from accelerometers and satellite orbit tracking. Though their computational complexity makes it difficult for them to be used for real-time operational orbit determination, such methods can provide density estimates that can be used to calibrate semi-empirical density models. The computational complexity of physics-based models can be reduced by representing them with a smaller subset of parameters using reduced order models [14, 15]. This technique has been used to demonstrate estimation of global atmospheric density by assimilating measurements from accelerometers [16], two-line element (TLE) data [17], and radar and GPS measurements [18]. All such data-assimilation methods are demonstrating significant improvements in global atmospheric density estimates over existing semi-empirical density models. But the obtained densities are uncertain to the ballistic coefficient estimated by the filter. Moreover, real-time tracking data from multiple sources is required to provide real-time density estimation which may prove to be a hurdle for implementation in operational use. A method that can estimate the local atmospheric density along the orbit simultaneously with the ballistic coefficient during orbit determination is needed for operational use by satellite operators.

The simultaneous estimation of density and drag-coefficient is complicated due to their highly correlated nature. In particular, a bias in the drag-coefficient and density cannot be simultaneously observed by the filter, as can be seen from the drag-equation, and will be estimated as a lumped term. Therefore, the cannonball drag-coefficient, estimated as a scale factor, not only averages out time-variations in the drag-coefficient due to attitude and ambient parameters but also absorbs time-averaged errors in the density model. Wright et al. [19] proposed a method to simultaneously estimate the drag-coefficient and density by modeling them as exponentially correlated Gauss-Markov processes. The drag coefficient is assumed to have a much slower variation than the density which allows separation of the two. This method provides a practical way to decorrelate the two parameters and has been used by McLaughlin et al. [20] to arrive at densities derived using CHAMP POD. But the bias terms in the density and drag-coefficient still cannot be estimated simultaneously, i.e., the estimate is inaccurate up to a constant bias. Moreover, high-frequency variations in the drag-coefficient due to attitude variations are not accounted for.

In this paper, we build on our previous work [21] on developing a method to estimate the drag-coefficient and the local atmospheric densities along the orbit by utilizing the time-variations in the drag-coefficient induced by changes in the satellite attitude. The higher-frequency variations in the drag coefficient can be estimated in the orbit determination using a Fourier series expansion in the body frame of the satellite. The Fourier series models, developed previously by the authors, have been shown to improve orbit determination and prediction for simulated and real data [22, 23]. The estimated Fourier coefficients contain information on gas-surface interaction (GSI) parameters that govern the drag-coefficient variation and can be used to invert specific uncertain parameters [24]. But the density was assumed to be perfectly known, and therefore, the estimated Fourier coefficients absorb any errors present in the density. The Fourier model for the drag-coefficient still might lead improvements in short-term orbit predictions if the estimated Fourier coefficients are able to emulate the combined variations in the drag-coefficient and density error [23]. But the Fourier coefficients themselves will not represent a true time-series of drag-coefficient. Therefore, the inverted GSI parameters will be physically inconsistent. But if the density error is modeled as a Gauss-Markov process, the higher-order Fourier coefficients (except the bias term) can be estimated simultaneously with the density corrections. In our previous work [21], we outlined a method to simultaneously estimate the higher-order Fourier coefficients with the density correction modeled as a second-order Gauss-Markov process. The Fourier coefficients are then used to invert uncertain GSI parameters. Once the GSI model is more accurately known, the drag-coefficient bias term can be calculated. An improvement in the estimated density and drag-coefficient with a few iterations of the method was demonstrated using synthetic data. Here, we validate the method using POD for the SPIRE satellites.

2. GAS-SURFACE INTERACTION MODELS (GSIMS)

The diffuse reflection incomplete accomodation (DRIA) model developed by by Walker et al. [25] based on the developments by Pilinksi et al. [26] is used in this work. The drag-coefficient of a flat plate with one side exposed to the flow is given by [25],

$$C_d = \frac{A}{A_{ref}}\left[\frac{e^{-\gamma^2 s^2}}{s\sqrt{\pi}} + \gamma\{1+\text{erf}(\gamma s)\}\left(1+\frac{1}{2s^2}\right) + \frac{\gamma}{2}r\left\{\gamma\sqrt{\pi}\{1+\text{erf}(\gamma s)\} + \frac{1}{s}e^{-\gamma^2 s^2}\right\}\right]. \tag{1}$$

where $\gamma = \cos\psi$, ψ being the angle between the unit vector normal to the plate and the velocity vector, A is the area of the plate, A_{ref} is a reference area, $\text{erf}(\gamma s)$ is the error function given by $\text{erf}(\gamma s) = \frac{2}{\sqrt{\pi}}\int_0^{\gamma s} e^{-t^2}dt$, r is the velocity ratio and s is the molecular speed ratio, defined as the ratio of the bulk speed (V_i) and the most probable speed of the gas molecules,

$$s = \frac{V_i}{\sqrt{\frac{2RT}{M}}} \tag{2}$$

where R is ideal gas constant, M is the mean molar mass and T is the ambient temperature. The velocity ratio, r, between the incident and reemitted particles is derived by Koppenwallner [27],

$$r = \sqrt{\frac{1}{2}}\sqrt{1+\alpha\left(\frac{4RT_s}{MV_i^2}-1\right)}. \tag{3}$$

where α is the energy accommodation coefficient and T_s is the temperature of the surface. Based on the work of Pilinski et al. [28, 26], the fraction of surface covered by atomic oxygen is estimated by a Langmuir isotherm as-

$$f = \frac{KP_0}{1+KP_0}. \tag{4}$$

where K is the Langmuir constant and P_0 is the partial pressure of atomic oxygen. The total drag-coefficient is then given by [25],

$$C_{D,T} = fC_{D,ads} + (1-f)C_{D,s}, \tag{5}$$

where $C_{D,ads}$ is the drag-coefficient for the surface covered by an adsorbate, assumed to exhibit diffuse reemission with complete accommodation ($\alpha = 1$). $C_{D,s}$ is the drag-coefficient based on molecular beam experiments on clean surfaces, computed using Goodman's formula for energy accommodation coefficient [29],

$$\alpha_s = \frac{K_s\mu}{(1+\mu)^2}, \tag{6}$$

where μ is the mass ratio between the atmospheric species and surface molecule. In this work, the mass of the surface molecule is assumed to be 65 amu while the mean molecular mass of the incoming atmospheric flow is satellite-position dependent. K_s is the substrate coefficient, also known as the Langmuir constant, that depends on the distribution of the incident particles [30]. For a plate perpendicular to the flow, the incident particle distribution is unidirectional and $K_s = 3.6$. For an inclined plate, the accommodation coefficient is given by,

$$\alpha_s = \frac{K_s\mu\cos\psi}{(1+\mu)^2}. \tag{7}$$

Therefore, $C_{D,ads} = C_d|_{(\alpha=1)}$ and $C_{D,s} = C_d|_{(\alpha=\alpha_s)}$.

3. BODY-FIXED FOURIER (BFF) MODEL

If the velocity vector rotates around a single axis in the body frame of the satellite, then the drag-coefficient can be expanded as a Fourier series around the angle of rotation (θ) as

$$C_d = \sum_{n=0}^{\infty}(\overline{\mathscr{A}}_n\cos n\theta + \overline{\mathscr{B}}_n\sin n\theta). \tag{8}$$

where the coefficients are given by,

$$\overline{\mathscr{A}}_n = \frac{1}{\pi}\int_0^{2\pi} C_d \cos n\theta d\theta, \tag{9}$$

$$\overline{\mathscr{B}}_n = \frac{1}{\pi}\int_0^{2\pi} C_d \sin n\theta d\theta, \tag{10}$$

for $n > 0$ and,

$$\overline{\mathscr{A}}_0 = \frac{1}{2\pi}\int_0^{2\pi} C_d d\theta, \tag{11}$$

and $\overline{\mathscr{B}}_0 = 0$ for $n = 0$.

It is possible to derive closed-form expressions for the body-fixed Fourier coefficients of a flat plate for the DRIA model that provide an explicit functional form of the Fourier coefficients in terms of the GSIM parameters [24].

4. MODELING DENSITY USING A GAUSS-MARKOV PROCESS

The dynamical model used in the estimation method can have structural errors and errors in governing parameters. Whereas some parameters can be estimated within the filtering framework, structural errors are more difficult to compensate for and can lead to filter divergence where the estimation error becomes larger than the covariance bounds. A common way to take the structural errors into account in the filter is to model them by the addition of noise. The dynamics equation with noise can be written as [31]

$$\dot{\boldsymbol{x}}(t) = \boldsymbol{A}(t)\boldsymbol{x}(t) + \boldsymbol{B}(t)\boldsymbol{u}(t) \tag{12}$$

The noise vector, $\boldsymbol{u}(t)$ is generally added to a subset of the states and therefore, of a smaller dimension than the state vector. In State Noise Compensation (SNC), white noise with a known covariance is used to compensate for the dynamics errors. Though SNC can prevent filter divergence by expanding the covariance bounds, it cannot capture the dynamics error since the noise parameters are not estimated. The use of Gauss-Markov processes to model the error known as Dynamic Model Compensation (DMC) allows the possibility of estimating it. A Gauss-Markov process is a correlated Gaussian noise such that the probability density function at the current time (t_n) depends on the probability density at the last time instant (t_{n-1}). The first-order Gauss Markov process (GMP1) is given by the first-order differential equation known as Langevin equation,

$$\dot{\eta}(t) = -\lambda\eta(t) + u(t) \tag{13}$$

where $E(u) = 0$ and $E[u(t)u(t+\tau) = Q\delta(\tau)]$. The Gauss-Markov process state, $\eta(t)$, is augmented with the state vector and estimated in the filter. The time constant or correlation time ($1/\lambda$) is a tuning parameter and needs to be calibrated. The first order Gauss-Markov process has been shown to be more accurate in compensating for errors in force models during orbit determination than simply adding white noise [32].

For dynamics errors with periodic components, a second-order Gauss-Markov process (GMP2) can prove to be more beneficial. The advantage of using a GMP2 over GMP1 has been demonstrated for gravity error compensation and the possibility of modeling other orbit-dependent errors such as atmospheric drag and solar radiation pressure using GMP2 was suggested [33]. In particular, using GMP2 to model the atmospheric density was proposed by Nievinski et al. [34] due to the oscillatory nature of the parameter. In the following, a framework to model errors in atmospheric density using a GMP2 with state noise is developed. The second order Gauss-Markov process can be represented in the state-space form as

$$\begin{bmatrix}\dot{x}_1\\ \dot{x}_2\end{bmatrix} = \begin{bmatrix}0 & 1\\ -\omega_n^2 & -2\zeta\omega_n\end{bmatrix}\begin{bmatrix}x_1\\ x_2\end{bmatrix} + \begin{bmatrix}0\\ c\end{bmatrix} w(t) \tag{14}$$

where $E(w) = 0$ and $E[w(t)w(t+\tau) = q\delta(\tau)]$. The natural frequency of the process (ω_n), the damping factor (ζ) and the strength of the white noise (c with $q = 1$) are tuning parameters that need to be calibrated. The calibration process can be performed by fitting the covariance of sample data for the modeled state to the autocovariance function of the GMP2. For example, in the case of density estimation, the sample data can be obtained from satellite missions

GRACE and CHAMP or datasets such as the SET HASDM database [35]. The autocovariance function is given by [33]

$$\psi_{nn}(\tau) = \frac{qc^2}{4\omega_n^3\zeta}\exp\left(-\zeta\omega_n|\tau|\right)\left(\cos\beta|\tau| + \frac{\zeta\omega_n}{\beta}\sin\beta|\tau|\right) \tag{15}$$

where $\beta = \omega_n\sqrt{1-\zeta^2}$. The covariance of the data samples can be fit to Eq. 15 with c, ζ and ω_n as the fitting parameters. The fitting process is detailed in Leonard et al. [33].

In the filter, x_1 and x_2 are both estimated and the correction to the modeled density is given by x_1. In addition to modeling the density correction using using a GMP2, a GMP0 correction to the density (bias with white noise) is estimated as well. The next section details the implementation of the algorithm in the filter.

5. SIMULTANEOUS ESTIMATION OF DENSITY AND DRAG-COEFFICIENT

During orbit determination, the drag-coefficient is usually estimated as part of the state vector since it is not accurately known apriori and its value can change in orbit. If the drag-coefficient was constant, it would not be simultaneously observable with the density bias since the filter would not be able to distinguish between two constant terms that exist in a product. Any correction to one term can be easily compensated for by the other term. Therefore, with an inaccurate constant drag-coefficient in the filter, the density can be estimated only up to a bias using the algorithm in the previous section. But for a satellite with attitude variations, the drag-coefficient will be time-varying as discussed in section "Body-fixed Fourier (BFF) model". Using the BFF model outlined in that section, the time-varying components of the drag-coefficient can be estimated simultaneously with the density. The bias term (zeroth order Fourier coefficient) still cannot be estimated due to the observability problem, but the higher order Fourier coefficients can be estimated simultaneously with the density corrections due to the time-varying attitude terms attached to them (Eq. 8). The bias in the drag-coefficient is primarily absorbed by the estimated density bias correction since the filter cannot distinguish between them. The estimated Fourier coefficients will also be affected but to a lesser extent since they govern higher-order frequencies in the drag-coefficient variation that cannot be captured by the bias. In order to calculate the drag-coefficient bias term, the functional relationship between the GSIM parameters and the Fourier coefficients derived in section 3 can be utilized. A few GSIM parameters with the largest uncertainty can be inverted from the estimated Fourier coefficients [24]. Then these inverted GSIM parameters can be used to calculate the bias term using the same equations for $n = 0$. The filter is re-initialized with the new bias term and everything else remaining the same. The new estimates of the Fourier coefficients from the filter will be more accurate due to a smaller bias in the filter and are used for the GSIM parameter inversion. The process is repeated a few times until the change in the bias term drops below a certain threshold.

The GSIM parameters can be inverted from the estimated Fourier coefficients using linearized least-squares. In this method, the estimated Fourier coefficients are the measurements and the GSIM parameter is the state to be estimated. The vector of Fourier coefficients have the following functional relation to the chosen GSIM parameter.

$$\boldsymbol{Y} = \boldsymbol{g}(X) \tag{16}$$

where $\boldsymbol{Y} = [\overline{\mathscr{A}}_1 ... \overline{\mathscr{A}}_n]^T$, X is the chosen GSIM parameter and $\boldsymbol{g} = [g_1 ... g_n]^T$, where g_k is the function that relates the k^{th} Fourier coefficient to the GSIM parameter. Note that the zeroth order Fourier coefficient is not part of the measurement vector since its estimate is not available. The following formulation demonstrates the inversion process for the fraction of surface covered by atomic oxygen in the DRIA model as denoted by Eq. 4.

The BFF coefficients depend on the fraction (f) as follows-

$$g_k = \left[f\overline{\mathscr{A}}_k|_{(\alpha=1)} + (1-f)\,\overline{\mathscr{A}}_k|_{(\alpha=\alpha_s)}\right]. \tag{17}$$

where $\overline{\mathscr{A}}_k$ are the analytical Fourier coefficients derived in the section "Body-fixed Fourier model". The least-squares algorithm requires the Jacobian of the measurement matrix. Therefore, $\boldsymbol{g}$ is linearized to obtain

$$\boldsymbol{G} = \left[\frac{\partial \boldsymbol{g_1}}{\partial f}, \frac{\partial \boldsymbol{g_2}}{\partial f}, ... \frac{\partial \boldsymbol{g_n}}{\partial f}\right]^T \tag{18}$$

where the k^{th} partial is given by

$$\frac{\partial \boldsymbol{g_k}}{\partial f} = \left[\overline{\mathscr{A}}_k|_{(\alpha=1)} - \overline{\mathscr{A}}_k|_{(\alpha=\alpha_s)}\right] \tag{19}$$

Therefore, the partials are Fourier expansions of the term in the square brackets. The least-squares estimate and its variance can then be found by iteratively solving the least-squares equation

$$x = (\boldsymbol{G}^T \boldsymbol{R}_f^{-1} \boldsymbol{G})^{-1} \boldsymbol{G}^T \boldsymbol{R}_f^{-1} \boldsymbol{y}_f \tag{20}$$

$$P = (\boldsymbol{G}^T \boldsymbol{R}_f^{-1} \boldsymbol{G})^{-1} \tag{21}$$

where x is the error in the estimate of the fraction at the current iteration, $\boldsymbol{y}_f$ is the measurement residual at the current iteration and $\boldsymbol{R}_f$ is the measurement noise covariance. The measurement noise covariance can be taken as the estimated covariance corresponding to the Fourier coefficients post orbit determination. The process can be repeated iteratively with the new estimate given by $f_{j+1} = f_j + x$, with j being the current iteration, until x drops below a fixed threshold. Once the estimate of the fraction is obtained, the bias term ($\overline{\mathscr{A}}_0$)can be calculated using the new fraction for $n = 0$. Any other uncertain GSIM parameter can be similarly inverted from the Fourier coefficient estimates.

The simultaneous estimation algorithm (Fig. 1) can be summarized as follows-

1. Initial values of the Fourier coefficients are obtained using the filter density model and GSIM parameter estimates.
2. The Kalman filter-smoother is initialized using these Fourier coefficients. In the filter, the zeroth-order Fourier coefficient or the bias term is kept constant while the higher-order Fourier coefficients are estimated simultaneously with the satellite position and velocity, and density DMC states.
3. The least-squares method outlined above is used to invert chosen GSIM parameters with the highest uncertainties from the estimated Fourier coefficients. The inverted values of the GSIM parameters are used to re-calculate the zeroth-order Fourier coefficient that becomes the new bias term for the Kalman filter-smoother with everything else remaining the same.
4. Steps 1-3 are repeated until the change in bias term drops below a chosen threshold. The bias in the density corrections due to the drag-coefficient will be significantly reduced.

6. SIMULATION RESULTS

In this section, the simultaneous estimation algorithm is tested through simulated scenarios. For all the cases, only the two-body gravitational force and atmospheric drag are considered in the force model. The true satellite trajectory is simulated using the parameters defined in Table 1. The initial errors in the states are assumed to be 10 m in position

Parameter		Value
Orbital elements	H	300 km
	i_0	65^0
	Ω_0	0^0
	u_0	0^0
Satellite parameters	m	500 kg
	A_{ref}	10 m^2
	Attitude	Inertially stabilized
Drag parameters	Drag-coefficient model	DRIA model
	Atmospheric Model	NRLMSISE-00

Table 1: Simulation parameters common for all the cases

and 10 cm in velocity in each direction. GPS measurements are generated for filter processing. The extended Kalman filter-smoother is iterated a few times to reduce linearization errors. All the estimates in the following results are smoothed estimates.

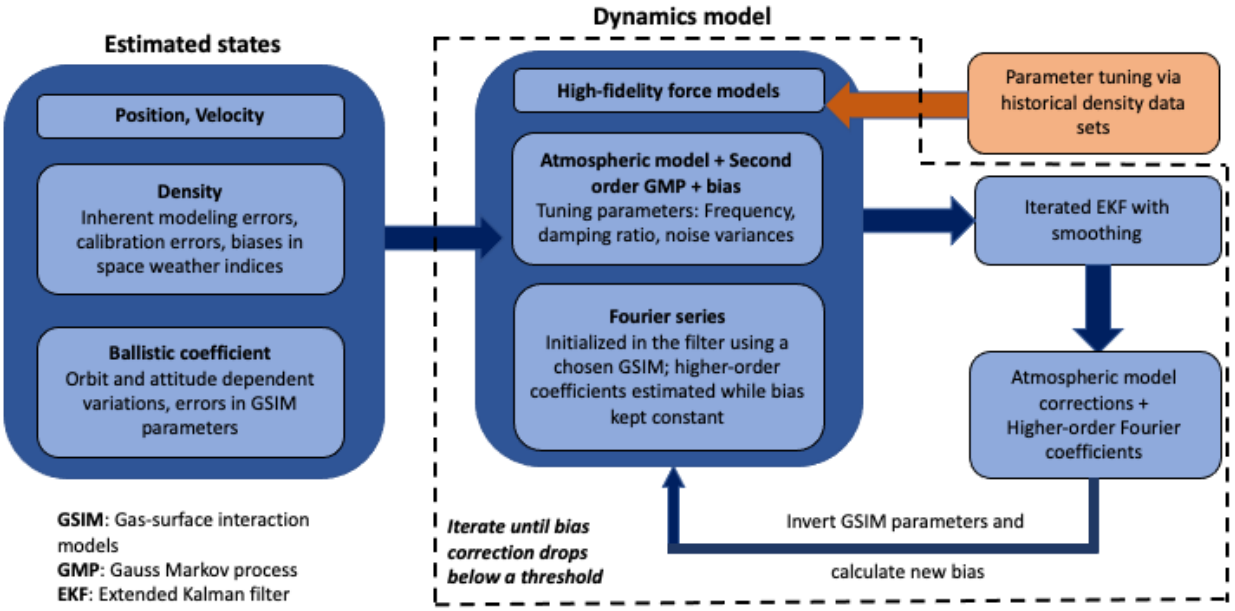

Fig. 1: Summary of the algorithm

In the filter, the atmospheric density is modeled using the JB2008 model and therefore is in error with the true density. The drag-coefficient is modeled using the BFF model with the coefficients initialized using diffuse reflection incomplete accommodation (DRIA) model in Eqs. 9-11. The GSIM parameters for the initialization process are assumed to contain errors and therefore, the initial Fourier coefficients are not known accurately and need to be estimated in the filter.

For the first case, the time period of Mar 23, 2007 is considered with quiet geomagnetic conditions and low solar activity. A one-day data-arc is processed in the filter which is iterated three times with bias updated after each iteration. The error in the drag-coefficient and density for each iteration is plotted in Fig. 2. The black curve in Fig. 2 (b) represents the true density correction which is the difference between the true density model (NRLMSISE-00) and filter density model (JB2008). It can be seen that the bias in both the drag-coefficient and density is reduced after each iteration. Note that the error in drag-coefficient should approach zero.

For the second case, the time period of Oct 28, 2003, also known as the Halloween storms due to extreme space weather disturbances, is considered. The density difference between NRLMSISE-00 and JB2008 is more than ten times the previous case. The algorithm is iterated twice to obtain the density and drag-coefficient estimates that are plotted in Fig. 3. The bias and root-mean-square (RMS) value of the drag-coefficient and density errors for each case are given in Table 2. The density bias is reduced by at least a factor of 10 after the final iteration.

7. APPLICATION TO REAL DATA

7.1 Dataset

The algorithm is tested on POD available for Spire satellites. Spire Global owns and operates a constellation of over 100 cubesats in the LEO regime with altitudes between 400-650 km and various inclinations. We have PODs for satellite IDs 83, 84 and 85 for 2018. The PODs were obtained (and made available to us) by processing GNSS pseudorange and carrier phase measurements using the RTOrb software in a Kalman filtering framework. The software considers non-spherical gravity up to degree and order 120, third-body perturbations from Sun and Moon, atmospheric drag with MSISe-90 as the density model and solar radiation pressure (SRP) with a cylindrical shadow model. Cannonball drag-coefficient and SRP coefficient are estimated within each arc. The PODs obtained by RTOrb have a precision of

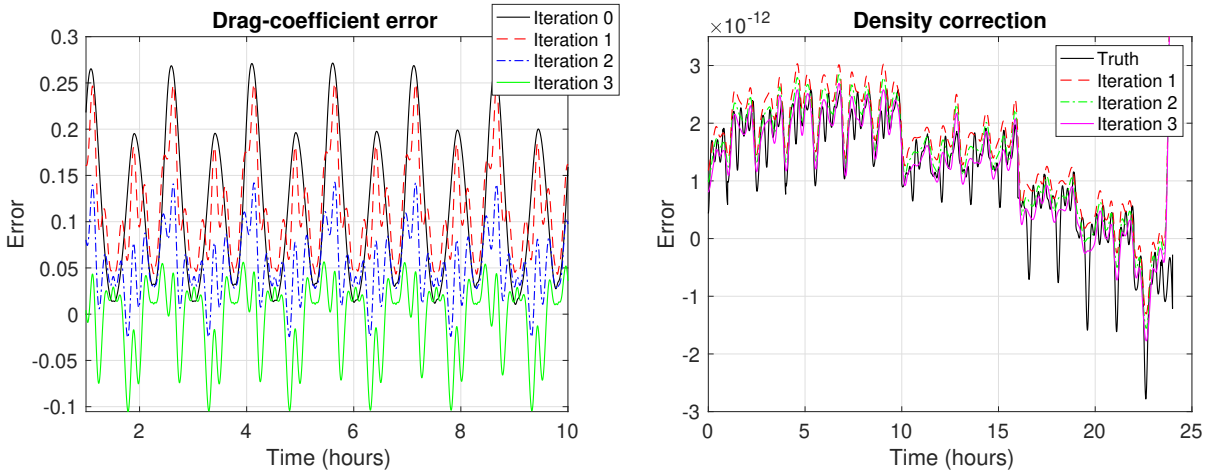

Fig. 2: Geomagnetically quiet conditions: (a) Drag-coefficient error after each iteration; (b) Density error after each iteration

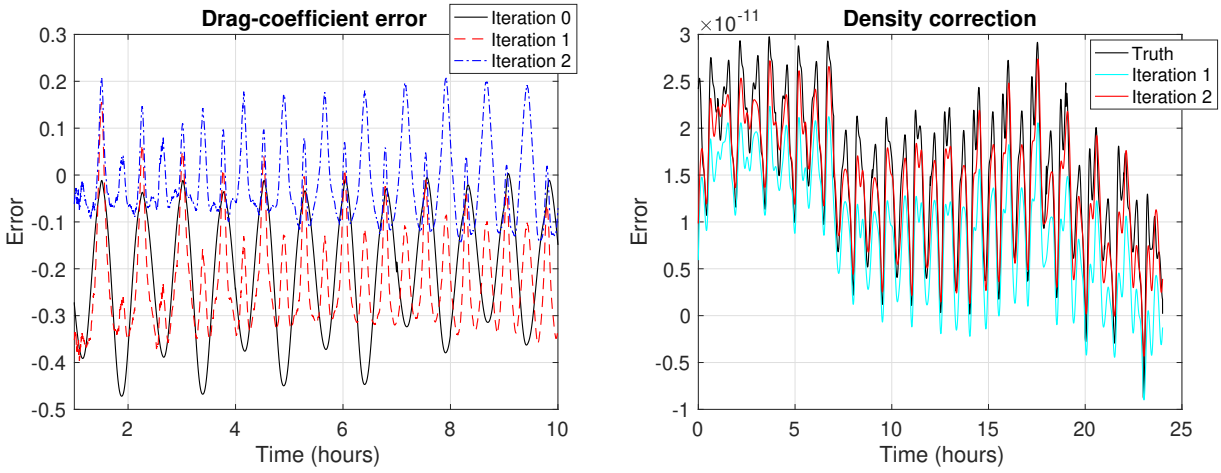

Fig. 3: Geomagnetically active conditions: (a) Drag-coefficient error after each iteration; (b) Density error after each iteration

Iteration	**Geomagnetically quiet**				**Geomagnetically active**			
	Drag coefficient error		Density error		Drag coefficient error		Density error	
	Mean	RMS	Mean	RMS	Mean	RMS	Mean	RMS
0	0.23	0.27	1.5e-12	1.6e-12	-0.37	0.46	1.7e-11	1.8e-11
1	0.22	0.24	-4.0e-13	5.1e-13	-0.46	0.5	6e-12	6.6e-12
2	0.1	0.12	-2.0e-13	3.6e-13	-0.03	0.2	1.3e-12	2.9e-12
3	-0.01	0.08	-1.6e-14	3.0e-13				

Table 2: Mean and RMS values of drag-coefficient and density errors after each iteration of the simultaneous estimation algorithm

several centimeters in position and sub-mm/s in velocity and are mostly available with a cadence of 1 s in data-arcs of 40-60 minutes. The attitude information of the satellites are also available in the form of quaternions between the body and the orbit frame. The quaternions are not uniformly available and can vary between a sample time of 10 s to 1000 s. For our application, the quaternions are needed as frequently as possible since the Spire satellites make frequent attitude maneuvers between an observing mode with the GNSS antennas aligned along-track and a power mode where the solar flux on the solar panels is maximized. Therefore, only a small subset of the data can be used for our applications. The POD and attitude data from Nov. 7, 2018 for satellite ID 83 is used in this work. The quaternions are interpolated to 1 s intervals using Spherical Linear IntERPolation (SLERP) [36]. As can be seen in Fig. 4, the velocity vector varies significantly and frequently in the x-y plane of the body frame. The variation out of the x-y plane is negligible.

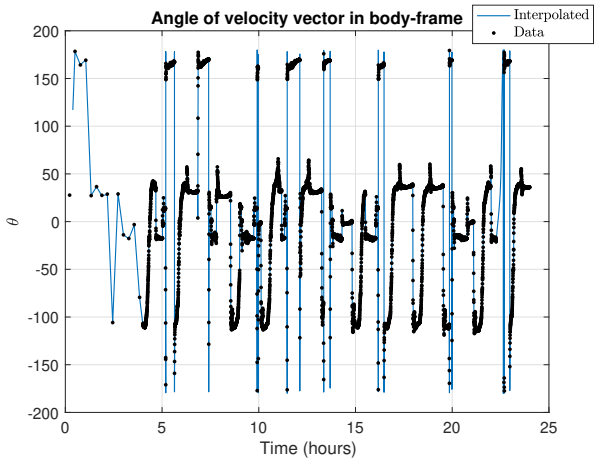

Fig. 4: Angle of velocity vector with body-x axis

7.2 Force model

A high-fidelity force model is required to propagate the Spire satellite orbits to be able to isolate the orbit determination residuals solely due to errors in atmospheric drag. The forces considered in the dynamics model are given in Table 3. The initial state from the POD for a given day is propagated with the different forces to analyze the relative contribution of each force to the orbital states. The POD is assumed to be the "truth" to compare the propagated orbit to.

Force	**Parameters**
Non-spherical gravity	EGM-2008 80X80
Third-body forces from Sun and Moon	DE-430 Ephemerides
Atmospheric drag	Density model - NRLMSISE-00, JB2008, SET HASDM densities Drag-coefficient- Cannonball, Panel (DRIA)
Solid Earth and Ocean tides	IERS 2010 Models [37]
Solar radiation pressure (SRP)	Cannonball, Panel
Relativistic correction	Post-Newtonian correction [38]

Table 3: Forces considered in propagation

The HASDM densities are obtained from the publicly available SET HASDM database [35]. The HASDM densities are available every 25 km altitude between 175-825 km with 3-h time resolution and $10^0 x 15^0$ latitude/longitude bins.

In order to use the densities in orbit determination, a multi-dimensional linear interpolation of the logarithm of the densities is performed over a grid of latitude, longitude, altitude and time.

The norm of the propagated position errors (w.r.t the POD) is plotted in the upper tile of Fig. 5 (a) for the major perturbing forces with different density models for drag in the propagator. A cannonball drag coefficient is used by averaging the predicted output from the DRIA model with input parameter values of $f = 1$ and $\alpha = 0.93$ [13] which results in a value of 0.23. The only other forces considered are non-spherical gravity (80x80) and third-body forces. HASDM performs a little better than JB2008 and both are significantly better than NRLMSISE-00, as expected. It should be noted that HASDM densities are available only every three hours and 25 km altitudes, therefore interpolated densities smooth out spatial and temporal variations at smaller scales. In the lower tile of Fig. 5 (a), the higher-fidelity forces are added one-by-one to the force model with HASDM as the density model. The addition of solid Earth tides and ocean tides leads to around 30 m improvement in the position at the end of the day and SRP improves it further by 25-30 m. Both the forces are non-negligible when trying to isolate orbit errors due to variations in the drag-coefficient. Adding the relativistic corrections leads to a small improvement of around 2 m and changing the gravity field to order 120 improves the error by less than a m which is barely discernible as shown in Fig. 5 (b).

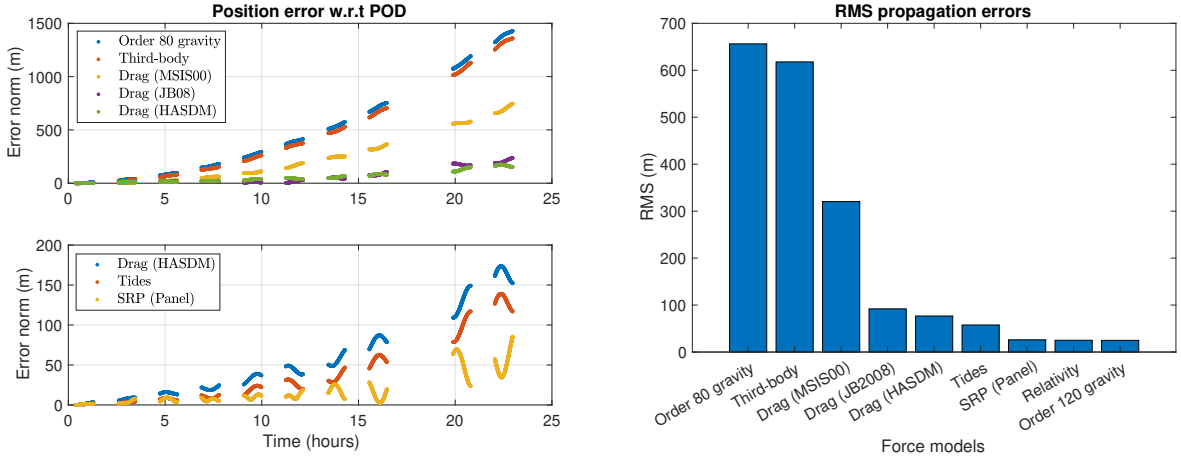

(a) (b)

Fig. 5: Propagation errors w.r.t POD: (a) Position errors with diffrenet forces added to the force model, (b) RMS of propagation errors with addition of each high-fidelity force to the dynamics.

In Fig. 5, the drag-coefficient is considered to be constant in the force model. But as seen in Fig. 4, the relative velocity vector varies significantly in the body frame of the satellite. The propagation error with the drag-coefficient modeled using DRIA with different values of f and α are compared in Fig. 6. From Fig. 6 (a), it would seem that drag-coefficient with $f = 0$ and $\alpha = 0.93$ would provide the most accurate drag-coefficient as the propagation errors are the smallest with these parameters and HASDM as the density model. But the propagation errors depend on the product of the density and drag-coefficient and it's quite possible that this particular drag-coefficient model is able to compensate for the lack of spatial and temporal resolution of HASDM densities to result in better propagation errors even though the drag-coefficient itself is less accurate. This can be seen from Fig. 6 (b) where the propagation error trends are quite different with NRLMSISE-00 as the density model and the same drag-coefficient values. The density and drag-coefficient values from the different models are plotted in Fig. 7. Note that the drag-coefficients are calculated with NRLMSISE-00 as the density model for the input ambient parameters to the DRIA model.

In the propagation, the SRP force model is assumed to be known accurately. The panel SRP force model is given by

$$\boldsymbol{a}_{SRP} = -P_s \frac{C_r}{m} \left(\frac{AU}{|\boldsymbol{r_s}|} \right)^2 f_s \sum_{k=1}^{6} A_k \cos\theta_k [(1-\rho_k)\hat{\boldsymbol{r}}_s + 2(\frac{\delta_k}{3} + \rho_k \cos\theta_k)\hat{\boldsymbol{n}}_{\boldsymbol{k}}]. \tag{22}$$

where $P_s = 4.56\ \mu Pa$ is the solar radiation pressure at 1 AU distance, $\boldsymbol{r_s}$ is the satellite to Sun position vector, f_s is the shadow factor [**?**], A_k are the areas of the satellite surfaces with $\hat{\boldsymbol{n}}_{\boldsymbol{k}}$ as the unit vectors in the satellite body frame, θ_k are the angles that the sun vector makes with the surface unit vectors, δ_k and ρ_k are the diffuse and specular reflectivities

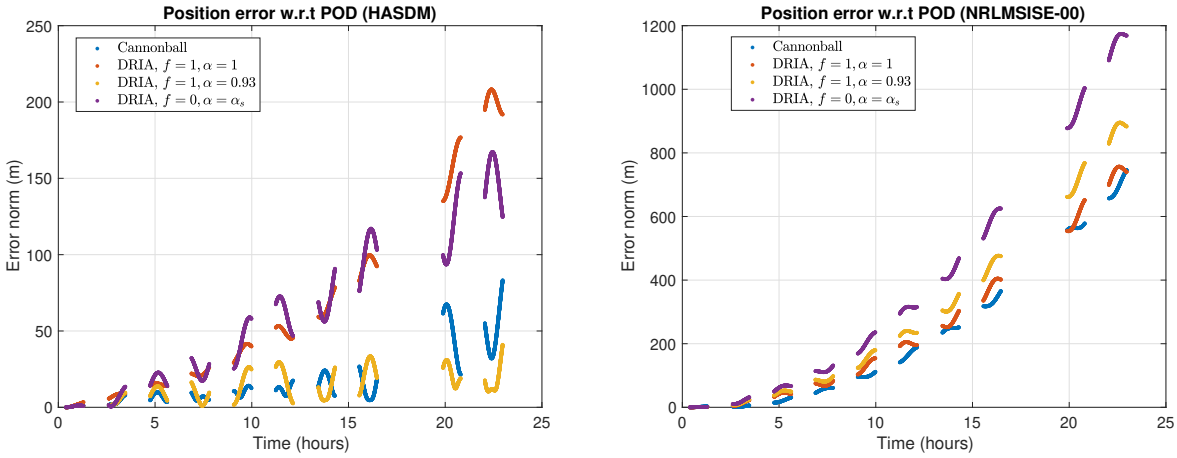

(a) (b)

Fig. 6: Propagation errors w.r.t POD with all forces and different drag-coefficient models with: (a) HASDM as the density model, (b) NRLMSISE-00 as the density model

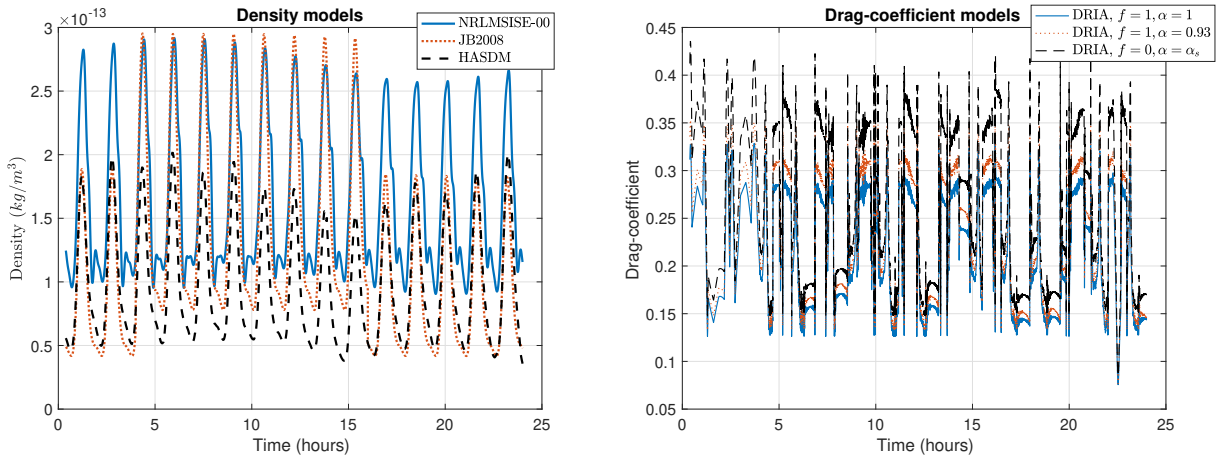

(a) (b)

Fig. 7: (a) Density values from different models, (b) Drag-coefficient values from different models

of the surfaces respectively and C_r is SRP coefficient or the scaling factor in the panel model. The available satellite properties are assumed to be accurate in the force model with $C_r = 1$. But it is instructive to compare the orbit determination residuals for a cannonball model and the given panel model with C_r being estimated in both cases to analyze if the given panel model is indeed closer to the truth. Therefore, The POD are processed in a batch filter with all the high-fidelity force models included in the dynamics and run for the two SRP models. The initial position and velocity, cannonball drag-coefficient and SRP coefficient are estimated with HASDM as the density model.

The position and velocity measurement residuals are plotted in Fig. 8. This can be further verified from Table 4 where the correction to the initial state (which is taken to be the initial POD state) is smaller for the panel model. It is good to note that for either model, the estimated drag-coefficient value is pretty much the same, i.e., the SRP errors don't alias [39] into the estimated drag-coefficient. The panel model with $C_r = 0.41$ is considered in the force model for the density inversion method.

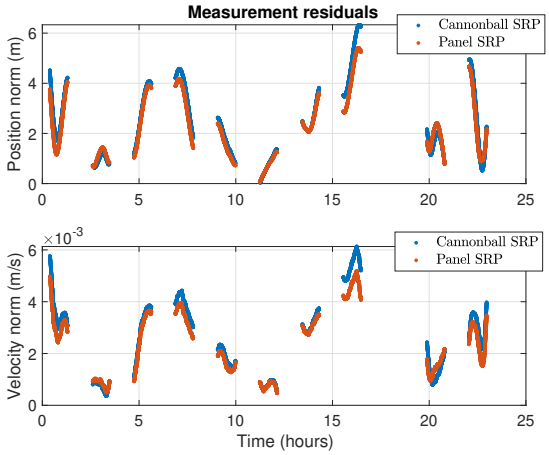

Fig. 8: Measurement residuals from batch processing of POD with two different SRP models

Parameter	Initial	Final	
		Cannonball SRP	Panel SRP
Norm of position error w.r.t POD (m)	0	4.522	3.766
Norm of velocity error w.r.t POD (m/s)	0	5.8e-3	5.0e-3
SRP coefficient	1	0.95	0.41
Drag-coefficient	0.23	0.262	0.259

Table 4: Initial and final estimates from the batch estimator for the two SRP models

In order to run the simultaneous estimation algorithm, initial estimates of the Fourier coefficients and their covariances need to be calculated. The Fourier coefficients are calculated using the expressions derived in Eqs. **??**-**??**. The standard deviations are calculated by considering the extremities of the range of variation of the GSIM input parameters. The fraction of surface covered by atomic oxygen (f) is assumed to vary from 0 to 1 and the accommodation coefficient of the covered surface is varied from 0 to 1. It is important to note here that the drag-coefficient and consequently, the body-fixed Fourier coefficients depend on ambient parameters that vary in the orbit. Ideally, a second Fourier series expansion in the orbit frame would be carried out to capture the periodic variations of the body-fixed Fourier coefficients [23]. But the orbit-fixed coefficients are highly correlated with density variations since both are dependent on similar sets of parameters which makes it difficult for them to be estimated simultaneously. Therefore, only the BFF coefficients are estimated in the filter as constants. The initial estimates of the body-fixed coefficients are calculated by averaging the GSIM in the orbit. The initial values are also dependent on the density model used to provide the GSIM parameter inputs such as the mean molecular mass. The Fourier coefficients are calculated using both NRLMSISE-00 and JB2008 for the input parameters to compare the dependence of the drag-coefficient on the density model. The effective initial drag-coefficient is calculated from the Fourier coefficients using Eq. 8. The relative error introduced in the drag-coefficient due to averaging of the Fourier series expansion $((C_{D,T} - C_{D,f})/C_{D,T})$is plotted in Fig. 9 (a) for extreme values of the GSIM parameters with NRLMSISE-00 as the density model. The relative error of the drag-coefficients calculated using JB2008 as the density model w.r.t the drag-coefficients calculated using NRLMSISE-00 as the density model is plotted in Fig. 9 (b). Both the averaging error and density model-dependent error are within 2 % when the accommodation coefficient is constant. But if the accommodation coefficient is modeled using Goodman's formula (Eq. 6), and therefore dependent on the density model, the relative errors are larger since now an additional parameter in the GSIM is tied to the density model.

The iterated EKF-smoother is run with the POD as measurements and NRLMSISE-00 as the density model. The state vector consists of the position, velocity, SRP coefficient, the density GMP2 states and the Fourier drag-coefficients.

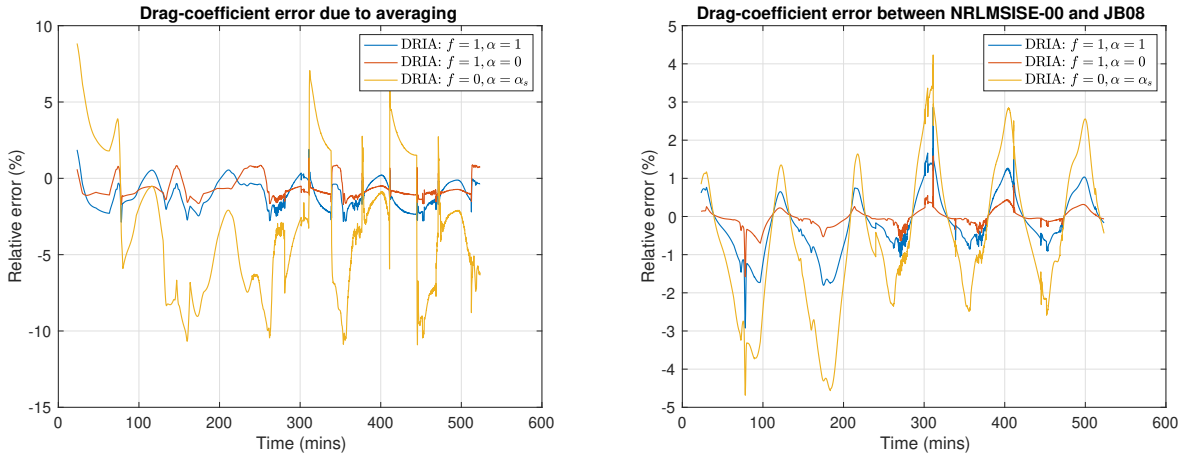

(a) (b)

Fig. 9: (a) Averaging error in the drag-coefficient, (b) Density model-dependent error in the drag-coefficient

Only the first and second order Fourier coefficients are estimated while rest of the coefficients till order 30 are kept constant in the filter. The tuning parameters for the GMP2 are found by fitting the autocovariance function in Eq. 15 to the error between NRLMSISE-00 and HASDM. The smoothed post-fit residuals after one iteration of the algorithm are less than a m in position as seen in Fig. 10 (a). But the estimated densities in Fig. 10 (b) are non-physical. The Fourier drag-coefficients are non-physical as well. The estimates are clearly absorbing other periodic unmodeled dynamics errors in the orbit due to the periodic nature of GMP2 modeling.

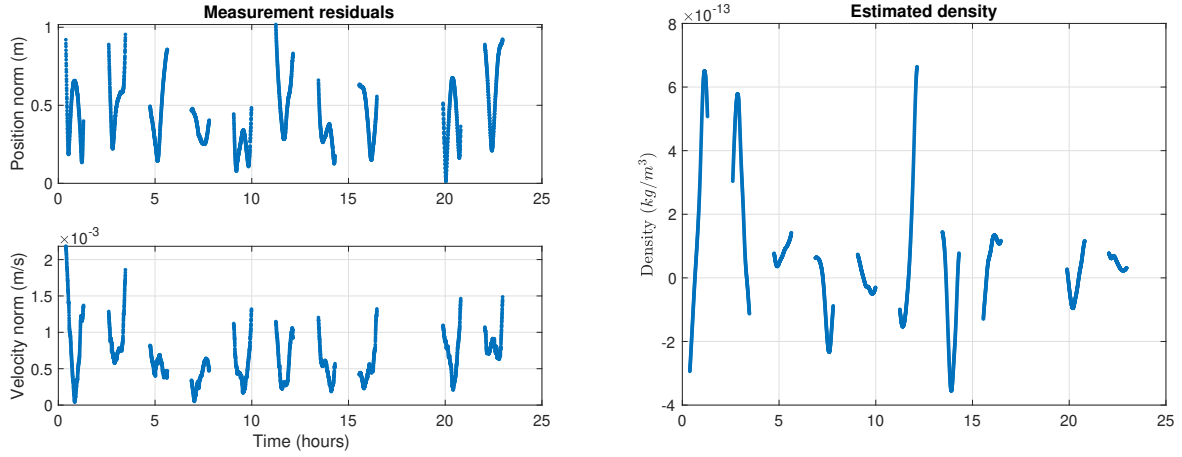

(a) (b)

Fig. 10: (a) Smoothed post-fit residuals, (b) Estimated densities from the iterated EKF-smoother

Therefore, the density correction model is changed to a GMP1 instead with the time constant taken as the orbital period which improves the density estimates as well as the Fourier coefficient estimates. The simultaneous estimation algorithm outlined in 5 iterated twice with the molecular ratio (r) in Eq. 3 inverted from the Fourier coefficient estimates. The post-fit residuals and the estimated densities from the two iterations are plotted in Fig. 11. It can be immediately noted that the estimated densities after each iteration move closer to HASDM, i.e., the algorithm is able to estimate the density bias. There's an improvement of about 30 % after the first iteration and 37 % after the second iteration in the density bias and error RMS. Although the estimated densities after both iterations are closer to the HASDM densities, the post-fit residuals are worse than Fig. 10. Even between the iterations, whereas the estimated density is closer to HASDM after the second iteration, the post-fit residuals are worse. This hints that there

are remaining unmodeled dynamics that are getting absorbed in the estimated densities and Fourier drag-coefficients. But even with the unmodeled errors, we are getting an improved estimate of the atmospheric density.

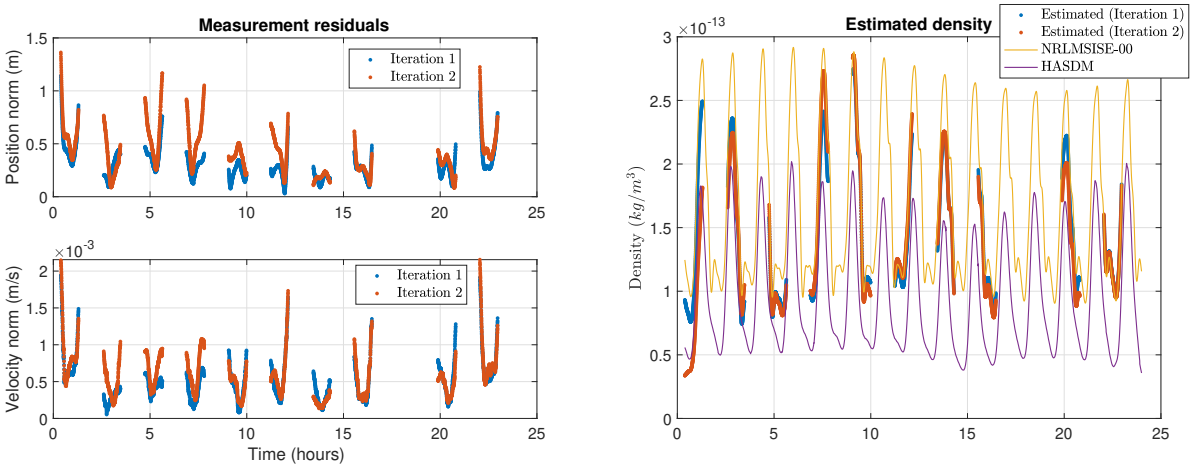

(a) (b)

Fig. 11: (a) Smoothed post-fit residuals, (b) Estimated densities from the iterated EKF-smoother

8. CONCLUSIONS

In this work, an algorithm to simultaneously estimate the density and drag-coefficient was developed. A second order Gauss Markov process along with a zeroth-order Gauss Markov process was utilized to model the density correction in the filter. For a satellite with a constant drag-coefficient, the density and drag-coefficient bias cannot be estimated simultaneously. But time time-variations in the drag-coefficient due to a changing satellite attitude allows the possibility of decorrelating the two. For a satellite with varying attitude, the time-variations in the drag-coefficient can be modeled using a body-fixed Fourier expansion. The higher-order Fourier coefficients can be estimated simultaneously with the density corrections. A few uncertain GSIM parameters can be inverted from the estimated Fourier coefficients in a least-squares methodology utilizing the functional relationship between them. The bias term can be re-calculated using the new GSIM parameter estimates and the process can be iterated a few times to get an unbiased density and drag-coefficient estimate. Through simulations, the improvement in estimating the density and drag-coefficient with this algorithm has been demonstrated for both geomagnetically quiet and active conditions. The bias in the drag coefficient and density was reduced by at least an order of magnitude for the cases considered here. The algorithm is validated using POD from Spire satellites. Even though the density correction modeled using a second-order GMP didn't converge on the truth, using a first order GMP allowed an improved estimate of the density. The NRLMSISE-00 density bias and error RMS w.r.t to HASDM are reduced by 30 % after the first iteration and 37 % after the second iteration. The poor density estimate with a GMP2 suggests unmodeled periodic dynamics remaining in the filter which needs to be further analyzed. Using the POD as measurements in the filter might introduce errors due to violation of the uncorrelated white measurement noise assumption in the Kalman filter. In the future, datasets with raw GPS measurements will be utilized for the validation. Machine-learning methods will be applied to train the tuning parameters of the Gauss Markov process over varying satellite orbits and atmospheric conditions using the SET HASDM database.

9. ACKNOWLEDGEMENTS

This work is funded by NASA's FINESST grant, number 80NSSC20K1508 and Kayhan Space Corp. We sincerely thank Eric Sutton, Senior Research Associate, SWx-TREC, CU Boulder, Shaylah Mutschler, Graduate Research Assistant, CCAR, CU Boulder and Penina Axelrad, Joseph T. Negler Professor, CCAR, CU Boulder for their time and effort in helping us process the Spire dataset. We would also like to thank Kent Tobiska, President, Space Environment Technologies (SET), for providing us the HASDM dataset.

10. REFERENCES

[1] Orbital Debris Research, Development Interagency Working Group of the National Science, and Technology Council. National Orbital Debris Research and Development Plan. Technical report, 2021.

[2] Jer-Chyi Liou and N.L. Johnson. Earth Satellite Population Instability: Underscoring the Need for Debris Mitigation. *National Aeronautics and Space Administration*, 2005.

[3] Salvatore Alfano, Daniel Oltrogge, Holger Krag, Klaus Merz, and Robert Hall. Risk assessment of recent high-interest conjunctions. *Acta Astronautica*, 184:241–250, 2021.

[4] M.D. Hejduk and D.E. Snow. The Effect of Neutral Density Estimation Errors on Satellite Conjunction Serious Event Rates. *Space Weather*, 16(7):849–869, 2018.

[5] National Research Council. *Continuing Kepler's Quest: Assessing Air Force Space Command's Astrodynamics Standards*. The National Academies Press, Washington D.C., 2012.

[6] David Perez and Ricardo Bevilacqua. Neural Network based calibration of atmospheric density models. *Acta Astronautica*, 110:58–76, 2015.

[7] J.M. Picone, A.E. Hedin, D.P. Drob, and A.C. Aikin. NRLMSISE-00 Empirical Model of the Atmosphere: Statistical Comparisons and Scientific Issues. *Journal of Geophysical Research*, 107(A12):2035–2051, 2002.

[8] Bruce R. Bowman, Kent W. Tobiska, Frank A. Marcos, Cheryl Y. Huang, Chin S. Lin, and William J. Burke. A New Empirical Thermospheric Density Model JB2008 Using New Solar and Geomagnetic Indices . *AIAA/AAS Astrodynamics Specialist Conference*, 2008.

[9] Sean Bruinsma. The DTM-2013 thermosphere model. *Journal of Space Weather and Space Climate*, 5(22), 2015.

[10] M.F. Storz, B.R. Bowman, M.J.I Branson, S.J. Casali, and W.K. Tobiska. High Accuracy Satellite Drag Model (HASDM). *Advances in Space Research*, 36:2497–2505, 2005.

[11] T. Matsuo, M. Fedrizzi, T.J. Fuller-Rowell, and M.V. Codrescu. Data assimilation of thermospheric mass density. *Space Weather*, 10(5):569–588, 2012.

[12] E.K. Sutton. A new method of physics-based data assimilation for the quiet and disturbed thermosphere. *Space Weather*, 10(5):736–753, 2018.

[13] E.K. Sutton, Jeffrey P. Thayer, Marcin D. Pilinski, Shaylah P. Mutschler, Thomas E. Berger, Vu Nguyen, and Dallas Masters. Toward Accurate Physics-Based Specifications of Neutral Density Using GNSS-Enabled Small Satellites. *Space Weather*, 19(6), 2021.

[14] P.M. Mehta and R. Linares. A methodology for reduced order modeling and calibration of the upper atmosphere. *Space Weather*, 15(10):1270–1287, 2017.

[15] P.M. Mehta and R. Linares. A new transformative framework for data assimilation and calibration of physical ionosphere-thermosphere models. *Space Weather*, 16(8):1086–1100, 2018.

[16] P.M. Mehta, R. Linares, and E.K. Sutton. A quasi-physical dynamic reduced order model for thermospheric mass density via Hermitian space-dynamic mode decomposition. *Space Weather*, 16(5):569–588, 2018.

[17] D.J. Gondalech and R. Linares. Real-time thermospheric density estimation via two-line element data assimilation. *Space Weather*, 18(2), 2020.

[18] D.J. Gondalech and R. Linares. Real-Time Thermospheric Density Estimation via Radar and GPS Tracking Data Assimilation. *Space Weather*, 19(4), 2021.

[19] James R. Wright and James Woodburn. Simultaneous Real-Time Estimation of Atmospheric Density and Ballistic Coefficient. Technical report, Analytical Graphics, Inc., 2004.

[20] C. A. McLaughlin, A. Hiatt, and T. Lechtenberg. Precision Orbit Derived Total Density. *Journal of Spacecraft and Rockets*, 48(1):166–174, 2011.

[21] Vishal Ray, Daniel J. Scheeres, Eric K. Sutton, and Marcin Pilinski. Density estimation using second-order Gauss-Markov processes. In *31st AAS/AIAA Spaceflight Mechanics Meeting*, number AAS 21-340, 2021.

[22] Vishal Ray, Daniel J. Scheeres, Siamak G. Hesar, and Matthew Duncan. A drag coefficient modeling approach using spatial and temporal Fourier expansions for orbit determination. *Journal of the Astronautical Sciences*, 67(3):1139–1168, 2020.

[23] Vishal Ray and Daniel J. Scheeres. A drag coefficient model to track variations due to attitude and orbital motion. *Journal of Guidance, Control and Dynamics*, 43(10):1915–1926, 2020.

[24] Vishal Ray, Daniel J. Scheeres, and Marcin Pilinski. Inverting gas-surface interaction parameters from Fourier drag-coefficient estimates. *Advances in space research*, 68(4):1902–1927, 2021.

[25] Andrew Walker, Piyush Mehta, and Joseph Koller. Drag Coefficient Model Using the Cercignani–Lampis–Lord Gas–Surface Interaction Model. *Journal of Spacecraft and Rockets*, 51(5):1544–1563, 2014.
[26] Marcin D. Pilinski, Brian M. Argrow, Scott E. Palo, and Bruce R. Bowman. Semi-Empirical Satellite Accommodation Model for Spherical and Randomly Tumbling Objects. *Journal of Spacecraft and Rockets*, 50(3):556–571, 2013.
[27] G. Koppenwallner. Energy Accommodation coefficient and Momentum Transfer Modelling. Technical Report HTG-TN-08-11, 2009.
[28] Marcin D. Pilinski, Brian M. Argrow, and Scott E. Palo. Semi-Empirical Model for Satellite Energy-Accommodation Coefficients. *Journal of Spacecraft and Rockets*, 47(6):951–956, 2010.
[29] Frank O. Goodman and Harold Y. Wachman. Formula for Thermal Accommodation Coefficient. M.I.T. Fluid Dynamics Research Laboratory Report, Massachusetts Institute of Technology, February 1966.
[30] Piyush M. Mehta, Craig A. McLaughin, and Eric K. Sutton. Drag coefficient modeling for grace using Direct Simulation Monte Carlo. *Advances in Space Research*, 52(12):2035–2051, 2013.
[31] Byron D. Tapley, Bob E. Schutz, and George H. Born. *Statistical Orbit Determination*, chapter 6. Elsevier Academic Press, 2004.
[32] Paul G. Constantine and Eric Dow. Dynamic Model Compensation for Near-Earth Satellite Orbit Determination. *AIAA Journal*, 13(3):343–349, 1975.
[33] Jason M. Leonard, Felipe G. Nievinski, and George H. Born. Gravity Error Compensation Using Second-Order Gauss–Markov Processes. *Journal of Spacecraft and Rockets*, 50(1):217–229, 2013.
[34] F. Nievinski, Brandon Yonko, and G. Born. Improved orbit determination using second-order gauss-markov process. *Advances in the Astronautical Sciences*, 140, 2011.
[35] K.W. Tobiska, B.R. Bowman, D. Bouwer, A. Cruz, K. Wahl, M. Pilinski, P.M. Mehta, and R.J. Licata. The SET HASDM density database. *Space Weather*, 2021.
[36] Ken Shoemake. Animating rotations with quaternion curves. In *SIGGRAPH '85: Proceedings of the 12th annual conference on Computer graphics and interactive techniques*, pages 245–254, 1985.
[37] Gérard Petit and Brian Luzum. IERS Conventions. IERS Technical Note No. 36, 2010.
[38] Olliver Montenbruck and Eberhard Gill. *Satellite Orbits: Models, Methods and Applications*, chapter 3.7.3, page 111. Springer, 2000.
[39] Vishal Ray and Daniel J. Scheeres. Gravitational Force-Model Aliasing with Non-Gravitational Force Coefficients in Dynamic Prediction. *Journal of Guidance, Control and Dynamics*, 43(10):1984–1997, 2020.